iScience

CellPress
OPEN ACCESS

Article

ZEB2 drives intra-tumor heterogeneity and skin squamous cell carcinoma formation with distinct EMP transition states

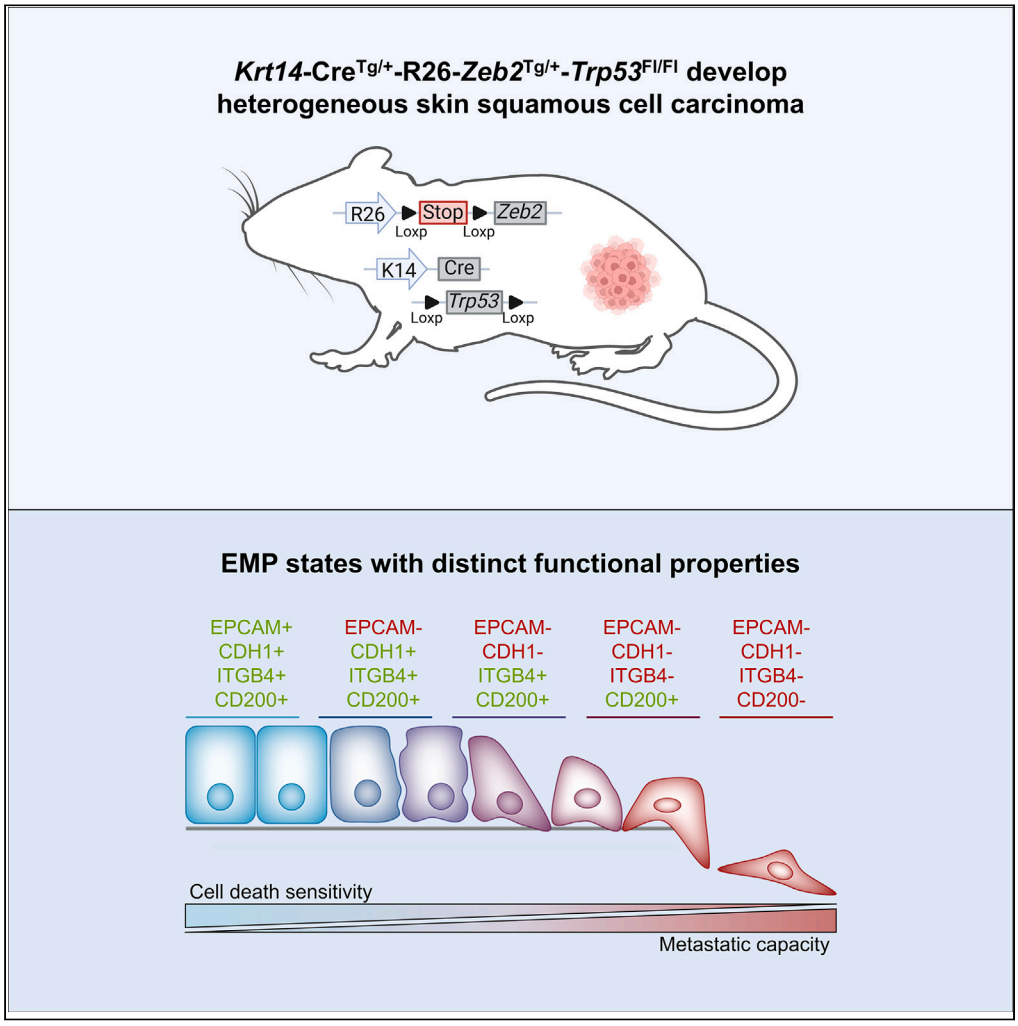

Jeroen Verstappe, Nicolas Skrypek, Jordy De Coninck, ..., Steven Goossens, Niels Vandamme, Geert Berx

geert.berx@ugent.be

Highlights

ZEB2 contributes to tumor initiation and heterogeneity in P53 knockout driven skin cancer

ZEB2^{+} skin tumors, show five EMT states based on EPCAM, CDH1, ITGB4, and CD200 markers

Mesenchymal states have higher metastatic capacity yet are more sensitive to cell death

Verstappe et al., iScience 27, 111169
November 15, 2024
https://doi.org/10.1016/j.isci.2024.111169

iScience

CellPress
OPEN ACCESS

Article

ZEB2 drives intra-tumor heterogeneity and skin squamous cell carcinoma formation with distinct EMP transition states

Jeroen Verstappe,[1,2] Nicolas Skrypek,[1,2] Jordy De Coninck,[1,2,3] Bieke Soen,[1,2] Joachim Taminau,[1,2] Marianthi Tatari,[1,2] Kenneth Bruneel,[1,2] Nele Loret,[1,2] Kato De Clercq,[1,2] Caroline Van den Broecke,[6,11] Koen Van De Vijver,[2,5,6,7] Jo Van Dorpe,[2,6] Jody Haigh,[8,9] Bram De Craene,[1,2] Steven Goossens,[2,10] Niels Vandamme,[1,2,3,4] and Geert Berx[1,2,12,*]

SUMMARY

About 5% of patients with cutaneous squamous cell carcinoma (cSCC) have a poor prognosis which is associated with a loss of tumor differentiation, invasion and metastasis, all of which are linked to the process of epithelial-to-mesenchymal plasticity (EMP). Here, we showed that the EMP-associated transcription factor ZEB2 drives cSCC heterogeneity which resembles biphasic carcinosarcoma-like tumors. Single cell RNA sequencing revealed distinct subpopulations ranging from fully epithelial (E) to intermediate (EM) to fully mesenchymal (M), associated with the gradual loss of cell surface markers EPCAM, CDH1, ITGB4, and CD200. Mesenchymal features were associated with a higher metastatic capacity and anoikis resistance, yet this comes with a sensitivity toward TNF-induced cell death. Altogether we provide insights in cSCC heterogeneity and modes to target mesenchymal-metastasis inducing cells.

INTRODUCTION

Skin cancer remains a growing global burden, accounting for one in three diagnosed cancers worldwide.[1] Among non-melanoma skin cancers, squamous cell carcinoma (SCC) is a prevalent subtype, with approximately 1.2 million new diagnoses in 2020.[2] While surgical excision provides long-term relapse-free survival for most patients, a small percentage of cases present with invasive or metastatic lesions that require alternative therapeutic interventions. Local recurrence and lymph node metastasis, invasion and poor differentiation occurs in approximately 5% of patients which poses a significant clinical burden due to the rapidly increasing incidence.[3–5] All these histopathological features have been linked to the epithelial-to-mesenchymal transition (EMT) process.

EMT is a process in which cells lose apical-basal polarity and cell-cell interactions and gain invasive and migratory capacities. EMT is essential during embryonic developmental stages, such as gastrulation and delamination of the neural crest yet can have devastating consequences upon activation in cancer.[6] Recently, it was shown that cells can present a range of epithelial and mesenchymal characteristics with regards to their degree of EMT which is known as the concept of epithelial-to-mesenchymal plasticity (EMP).[7–12] EMP implies that cancer cells can present as a spectrum of functionally distinct cellular states which consequently contribute to a higher intra-tumor heterogeneity. It is driven by several transcription factors including ZEB2 that downregulate epithelial gene expression of e.g., E-cadherin, EpCAM, and keratins and upregulate mesenchymal gene expression of e.g., vimentin, fibronectin, and matrix metalloproteases.[13–15]

In our study we investigated the role of ZEB2-driven EMP in cutaneous squamous cell carcinoma (cSCC) heterogeneity. For this we used the previously published *Krt14Cre*$^{Tg/+}$-*Trp53*$^{Fl/Fl}$ mice[16] as *Trp53* is the most commonly mutated gene in cSCC[17] and a *Zeb2*-transgenic mouse to induce ZEB2-mediated EMT in a *Trp53* KO background. We aimed to further unravel EMP states driven by ZEB2 and explore their functional properties.

[1]Molecular and Cellular Oncology Laboratory, Department of Biomedical Molecular Biology, Ghent University, Technologiepark 71, 9052 Ghent, Belgium
[2]Cancer Research Institute Ghent (CRIG), Ghent, Belgium
[3]VIB Single Cell Core, VIB, Ghent-Leuven, Belgium
[4]VIB-UGent Center for Inflammation Research, Technologiepark 71, 9052 Ghent, Belgium
[5]Department of Pathology, The Netherlands Cancer Institute, Amsterdam, the Netherlands
[6]Department of Pathology, Ghent Unviversity Hospital, Ghent, Belgium
[7]Department of Pathology, Antwerp University Hospital, Antwerp, Belgium
[8]Department of Pharmacology and Therapeutics, Rady Faculty of Health Sciences, University of Manitoba, Winnipeg, MB, Canada
[9]Paul Albrechtsen Research Institute, CancerCare Manitoba, Winnipeg, MB, Canada
[10]Department of Diagnostic Sciences, Ghent University, Ghent, Belgium
[11]AZ Sint-Lucas Gent, Ghent, Belgium
[12]Lead contact
*Correspondence: geert.berx@ugent.be
https://doi.org/10.1016/j.isci.2024.111169

RESULTS

ZEB2 expression in the skin causes mixed- or mesenchymal-like squamous cell carcinoma

To study the effect of EMP in cSCC, we crossed the previously described *Krt14Cre*$^{Tg/+}$-*Trp53*$^{Fl/Fl}$ (P53 KO) with *Krt14Cre*$^{Tg/+}$-*Rosa26-Zeb2*$^{Tg/Tg}$ (ZEB2 Tg) mice to obtain *Krt14Cre*$^{Tg/+}$ -*Rosa26-Zeb2*$^{Tg/+}$/*Trp53*$^{Fl/Fl}$ (P53 KO ZEB2 Tg) mice which express a bicistronic transcript encoding *Zeb2* and enhanced green fluorescent protein (eGFP) in a *Trp53* knockout background[16,18] (Figure 1A). This eGFP expression allows sensitive *in vivo* Cre recombinase-mediated cell tracking of ZEB2-transgenic cells.

We previously showed that constitutive expression of ZEB2 in cells originating from the KRT14+ basal epidermal layer causes hair loss and sporadic crusty skin on non-hairy body parts (e.g., ears and nose) from the onset of 10 weeks.[18] Morphological analyses of the skin identified a hyperproliferative basal skin layer with attenuated expression of tight junctional proteins (e.g., Occludin) yet these mice never developed cancerous lesions. Similarly, P53 KO ZEB2 Tg, but not P53 KO mice show increased epidermal thickness due to hyperproliferation (Figures 1B, 1C, and S1A).

P53 KO mice developed both skin- and mammary gland tumors at low frequency with long latency (60 weeks [$N = 20$]) (Figure 1D). These skin lesions were histologically identified as papillomas or SCC with a completely epithelial phenotype (Figures 1E–1G). Indeed, keratin 14 (KRT14), a well-defined epithelial marker was strongly expressed by cancer cells whereas vimentin (VIM) was restricted to infiltrating fibroblasts (Figure S1B). In this mouse model, ectopic ZEB2 expression caused significantly faster tumor initiation (37 weeks [$N = 49$], $p < 0.001$) and almost exclusively resulted in skin cancerous lesions (Figures 1D and 1E). Histological analyses showed that these skin tumors exhibited a very strong loss of epithelial differentiation, ranging from lesions with a mixed epithelial-mesenchymal phenotype to a fully mesenchymal phenotype (Figures 1E and 1F). This was confirmed through co-immunostaining of KRT14-VIM and CDH1-VIM, illustrating a spectrum of tumors ranging from mixed epithelial-mesenchymal to fully mesenchymal (Figures 1G and S1C). Moreover, the presence of GFP based fate mapping confirmed that mesenchymal-like cancer cells originated from a KRT14+ epithelial progenitor. Interestingly, one P53 KO mouse had an undifferentiated skin tumor with a CDH1^{low}VIM^{high} phenotype (Figure S1D). This tumor showed strong, endogenous expression of ZEB2 in the nuclei of the cancer cells, in contrast to the other epithelial differentiated P53 KO skin tumors, where ZEB2 was absent or restricted to infiltrating fibroblasts (Figure S1D). As many of these epithelial-mesenchymal mixed lesions showed resemblance with carcinosarcomas, we performed ZEB2 immunostainings on human skin carcinosarcomas which showed high expression of this EMP-associated transcription factor (Figure 1H). Since carcinosarcomas of the skin are exceedingly rare, we aimed to extend our findings to the more frequently encountered gynecological carcinosarcomas. We observed that these tumors also exhibited high ZEB2 expression within their sarcoma-like compartments (Figure 1H). These tumors also displayed pan-cytokeratin and vimentin positive regions in the carcinoma and sarcoma-compartment respectively (Figure S1E).

Single cell RNA sequencing reveals intra- and inter-tumor heterogeneity in P53^{KO}/ZEB2-driven skin lesions

To further characterize the observed ZEB2 driven intratumor heterogeneity, we performed single cell RNA sequencing (scRNAseq) on GFP sorted cancer cells from different spontaneous tumors derived from a mesenchymal-like tumor (annotated MSL) and a tumor with a mixed epithelial-mesenchymal phenotype (annotated MIX) using the GemCode single-cell platform (10x Genomics). This scRNAseq analysis was used to subclassify P53 KO ZEB2 Tg tumors on the molecular level into MIX and MSL cancerous lesions. Unsupervised clustering was performed on the integrated dataset generating 11 Uniform Manifold Approximation and Projection (UMAP) clusters tumor (Figure 2A). Based on differentially expressed genes (DEGs) and epithelial (*Krt6a*, *Trp63*, *Krt5*) and mesenchymal (*Pdgfrb*, *Hmga2*) cell identity markers we were able to identify both epithelial and mesenchymal-like differentiation in the MIX tumor whereas epithelial cells were completely absent in the MSL tumor (Figures 2A–2D). Within the epithelial cell cluster, comprising cells uniquely from the MIX tumors, we identified cells with enhanced proliferative and ECM remodeling expression signatures (EPI_PROL and EPI_ECM, respectively). However, this epithelial cluster also contained cells which were strongly differentiated (EPI_DIF) marked by the highest expression of several epithelial markers (*Krt17*, *Sfn*, and *Krt6a*). Several epithelial markers (*Krt6a*, *Krt5*, and *Sfn*) demonstrated a gradient expression pattern, ranging from the most epithelial to the mesenchymal clusters suggesting an ongoing plasticity between transitional states (Figure 2D).

Within the malignant mesenchymal-like cell cluster, we further defined a proliferative subcluster MES_PROL (marked by *Mki67*, *Pcna*, and *Cenpa*), and an extracellular matrix (ECM) remodeling cluster MES_ECM (marked by *Col5a1*, *Col3a1*, *Mmp2*, and *Mmp13*) consisting of cells from both MIX and MSL tumors. This implies the emergence of functionally similar (proliferative, ECM remodeling) cell types in MIX and MSL tumors. However, one additional cluster, MES_IMS showed upregulation of several cytokines (*Ccl2*, *Ccl5*, and *Cxcl1*) indicating that inter-tumor heterogeneity might be partly driven by the tumor microenvironment (Figures 2A–2D).

Epithelial-mesenchymal mixed cSCC lesions exhibit a snapshot of EMP with epithelial, intermediate, and mesenchymal subpopulations

Cancer cells derived from an epithelial-mesenchymal mixed cSCC that were GFP sorted and cultured *in vitro* retained both their epithelial and mesenchymal features with cuboid-like cells (epithelial) forming compact islands surrounded by spindle-shaped cells (mesenchymal-like). We confirmed that early passage cell-cultures range from epithelial-mesenchymal mixed to mesenchymal-like through RT-qPCR for epithelial and mesenchymal markers and immunofluorescence for KRT14 and VIM (Figures 3A and 3B).

To further validate whether cancer cells maintained their epithelial-mesenchymal mixed phenotype *in vitro*, we performed scRNAseq on an early passage derived cell culture, identifying 8 UMAP clusters (Figure 3C). Since these cultured cells were inherently proliferative and lacked a tumor microenvironment (TME), the TME and proliferation-related signatures observed *in vivo* were absent in our *in vitro* dataset. However

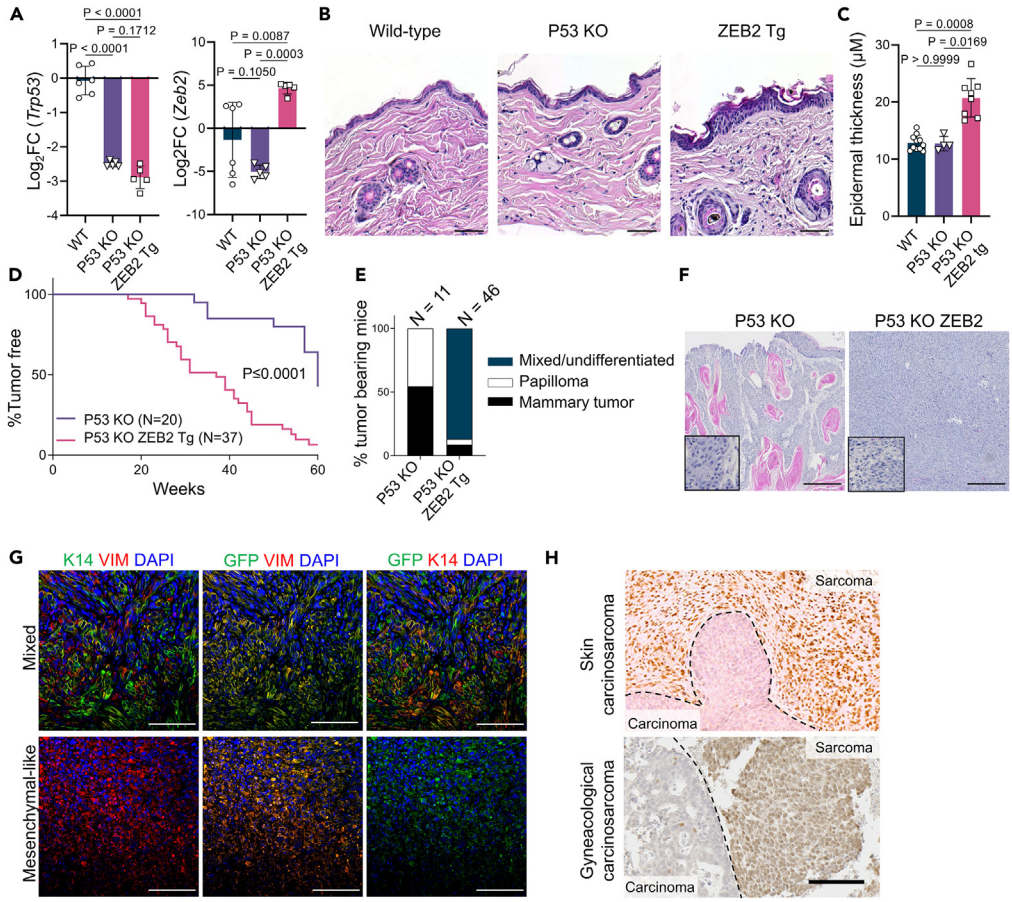

Figure 1. ZEB2 expression in the skin causes epithelial-mesenchymal mixed- or mesenchymal-like squamous cell carcinoma

(A) Gene expression of *Trp53* and *Zeb2* of back skin from tumor bearing P53 KO (*K14Cre*$^{Tg/+}$-*Trp53*$^{Fl/Fl}$) ($N = 5$) and P53 KO ZEB2 Tg (*K14Cre*$^{Tg/+}$-*R26-Zeb2*$^{Tg/+}$-*Trp53*$^{Fl/Fl}$) ($N = 5$) mice and age-matched wild-type ($N = 6$) littermates. Statistical significance was determined with a one-way Anova followed by a Tukey's test. Data are represented as mean ± SD.

(B) H&E sections of representative wild-type, of P53 KO (*K14Cre*$^{Tg/+}$-*Trp53*$^{Fl/Fl}$) and P53 KO ZEB2 Tg (*K14Cre*$^{Tg/+}$-*R26-Zeb2*$^{Tg/+}$-*Trp53*$^{Fl/Fl}$) mice. Scale bar, 50 µM.

(C) Epidermal thickness of wild-type ($N = 11$), of P53 KO (*K14Cre*$^{Tg/+}$-*Trp53*$^{Fl/Fl}$) ($N = 4$) and P53 KO ZEB2 Tg (*K14Cre*$^{Tg/+}$-*R26-Zeb2*$^{Tg/+}$-*Trp53*$^{Fl/Fl}$) ($N = 8$) mice. Statistical significance was determined using a kruskal wallis test followed by a Dunn's multiple comparisons test. Data are represented as mean ± SD.

(D) Tumor-free survival curve (Kaplan-Meier) of P53 KO (*K14Cre*$^{Tg/+}$-*Trp53*$^{Fl/Fl}$) ($N = 20$) and P53 KO ZEB2 Tg (*K14Cre*$^{Tg/+}$-*R26-Zeb2*$^{Tg/+}$-*Trp53*$^{Fl/Fl}$) ($N = 37$) mice. Once a tumor was palpable (skin/mammary gland), the mouse was considered tumor positive. Statistical significance was determined via the log rank Mantel-cox test.

(E) Histogram of the cancer type and differentiation phenotype of tumors developed in P53 KO and P53 KO ZEB2 Tg mice.

(F) Hematoxylin and eosin staining of skin tumor sections of P53 KO and P53 KO ZEB2 Tg mice.

(G) Co-immunostaining for eGFP, Vimentin (VIM) and keratin 14 (KRT14) on skin tumor sections of P53 KO and P53 KO ZEB2 Tg mice. Scale bar, 100 µM.

(H) Immunostaining for ZEB2 in a human skin carcinosarcoma and gynecological carcinosarcoma. Scale bar, 100 µM.

similar to the MIX *in vivo* tumor, the expression of epithelial genes showed a gradient expression pattern transitioning from fully epithelial to mesenchymal (Figure S2A). Moreover, there were strongly conserved epithelial and mesenchymal markers present, indicating that EMP related gene signatures were preserved during cell culturing. These findings provide an accessible model for studying the regulation and functional role of EMP in cSCC development and maintenance.

Based on the *in vitro* scRNAseq dataset we were able to identify a defined set of cell surface markers for the different cell populations with graded epithelial to mesenchymal differentiation states: CD200+ITGB1+CDH1+EPCAM+ (EPCAM+), CD200+ITGB4+CDH1+EPCAM- (CDH1+), CD200+ITGB4+CDH1-EPCAM- (ITGB4+), CD200+ITGB4-CDH1-EPCAM- (CD200+), and CD200-ITGB4-CDH1-EPCAM- (CD200-) (Figures 3D and 3E). In our *in vivo* MIX tumor scRNAseq dataset, both *Itgb4* and *Cd200* expression followed a similar expression pattern as seen *in vitro*. However, while *Cdh1* and *Epcam* expression was very low in this dataset they were detected *in vivo* through immunofluorescence (Figures S2B and S2C). We could further show these cell surface markers correlate well with our previous observations that early passage derived cell cultures display a range of EMP phenotypes (Figures 3B and 3F, Table S1). This stepwise transition was visualized by further subclustering our single cell dataset based on expression of the aforementioned markers followed by PCA (Figure S2D). To validate our

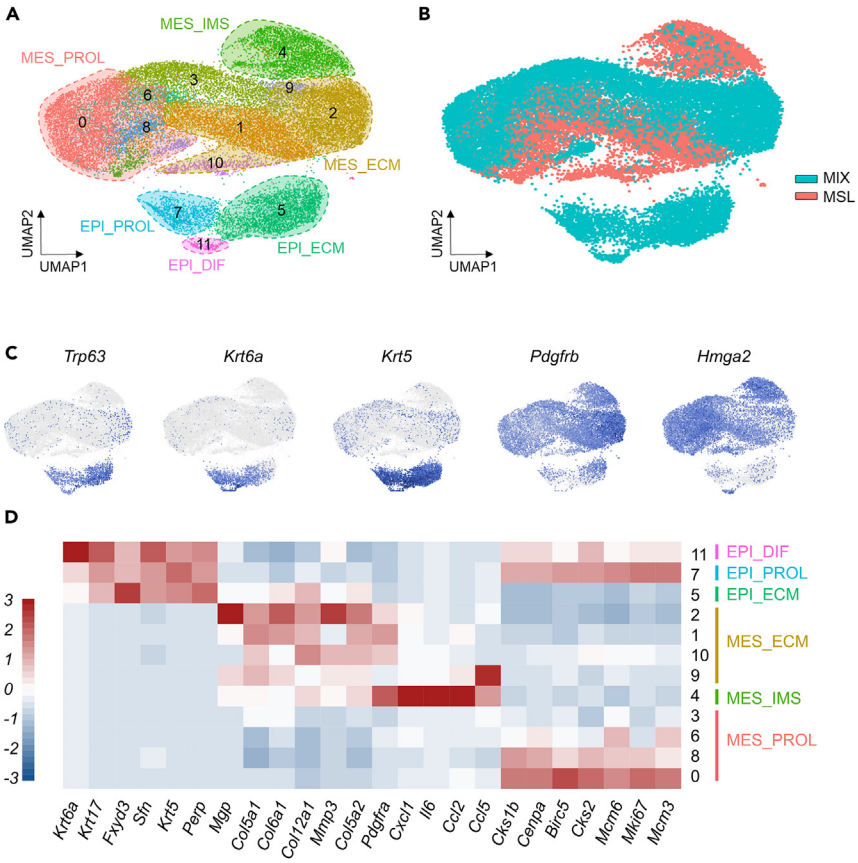

Figure 2. Single cell RNA sequencing reveals intra- and inter-tumor heterogeneity in P53KO/ZEB2 Tg-driven skin lesions

(A) The integration of single cell RNA sequencing performed on GFP sorted cells from a mixed (MIX) and mesenchymal-like (MSL) tumor revealed 11 UMAP clusters.

(B) Distribution of the MIX and MSL clusters within the integrated UMAP.

(C) Expression of indicated epithelial and mesenchymal markers by cell clusters.

(D) Heatmap showing the expression of epithelial and mesenchymal markers by different cell clusters.

findings in a second model, we used the published dataset from *Lgr5-cre*^{ER};*Kras*^{G12D};*Trp53*^{cKO};*Rosa-YFP* (LKPR) mice which develop mixed tumors.[19] Here, our identified cell surface markers also correlate with the epithelial compartment whereas cells high in mesenchymal markers are CD200- (Figure S2E).

To validate this stepwise transition between an epithelial and mesenchymal differentiation state, cancer cells were fluorescence-activated cell sorted (FACS) based on the aforementioned cell surface markers and immunostained on cytospin against keratin 14 (KRT14) and vimentin (VIM). This confirmed the existence of KRT14+VIM-, KRT14+VIM+, and KRT14-VIM+ cells supporting a graded loss and gain of epithelial and mesenchymal markers, respectively (Figures 4A–4C). Moreover, RT-qPCR for well-known epithelial markers (*Cldn4*, *Cldn7*, *Cdh1*..) or keratinocyte markers (*Krt14*, *Krt5*..) confirmed a stepwise loss from epithelial to mesenchymal (Figures 4C, S2F, and S2G). Similarly, well known mesenchymal markers (*Vim*, *Cdh2*..) and matrix-remodeling related genes (*Mmp3*, *Col6a1*..) showed a stepwise gain in expression (Figures 4C, S2F, and S2G). Taken together these results demonstrate that ZEB2-driven EMP in mixed cSCCs progresses through several cellular states spanning from fully epithelial to intermediate to mesenchymal.

The degree of EMP dictates functional properties in cSCC tumor cells

Since the process of EMT has been demonstrated to be crucial for tumor metastasis by aiding cancer cells in surviving in the bloodstream,[20] we initially examined anoikis resistance by growing epithelial-mesenchymal mixed cSCC cells on low-adherence plates or normal cell culture plates. In these heterogeneous cell cultures, seeding these cells in low-adherence plates caused a shift toward a more mesenchymal phenotypes and a decrease in fully differentiated EPCAM+ cells. This is in accordance with previously reported results that show that mesenchymal and intermediate states survive better in circulation[21–23] (Figure 5A). Since anoikis resistance is an important hallmark of metastasis, EMP subpopulations were sorted and injected in the tail-vein of NOD/SCID/IL2Rγ null (NSG) mice. In contrast to recent studies where early hybrid EMP phenotypes exhibited a higher metastatic capacity, we showed that mice injected with cells harboring mesenchymal features show the worst

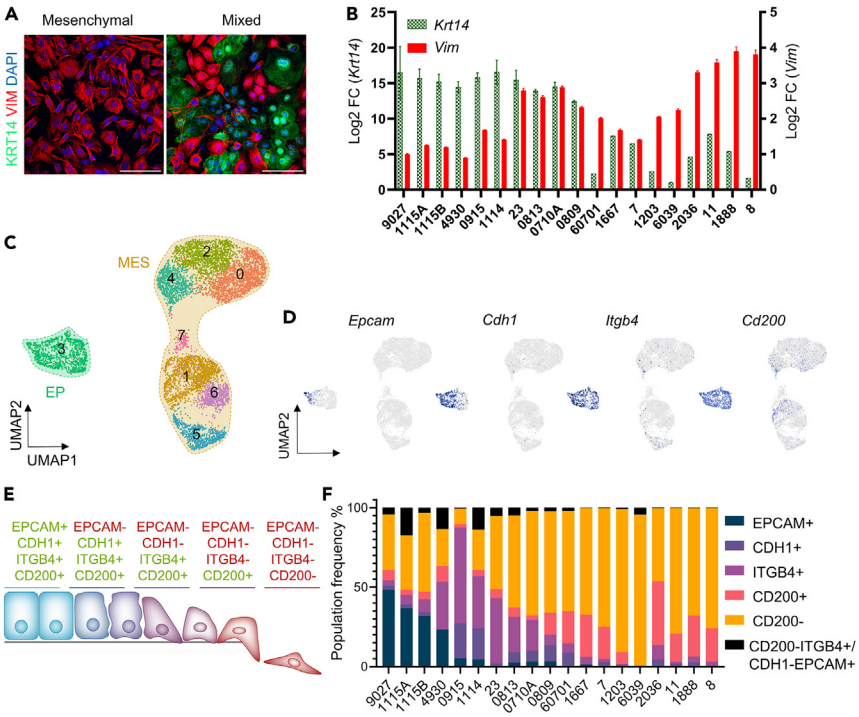

Figure 3. P53KO ZEB2Tg cSCC cells maintain intra-tumor epithelial heterogeneity upon cell culturing

(A) Early passage cell cultures derived from mixed tumors showed both KRT14+ and VIM+ cells whereas cells derived from mesenchymal-like tumors cells only showed VIM+ cells *in vitro*. Scale bar = 100 μM.

(B) RT-qPCR for *Vim* and *Krt14* showed that early-passage cell cultures derived from *K14Cre*$^{Tg/+}$-*R26-ZEB2*$^{Tg/+}$-*Trp53*$^{Fl/Fl}$ mouse tumors display a range of epithelial and mesenchymal phenotypes. Technical triplicates were used.

(C) UMAP showing 8 clusters obtained using single cell RNA sequencing on an early passage cell culture derived from a mixed cSCC.

(D) Expression of *Epcam*, *Cdh1*, *Itgb4*, and *Cd200* in our scRNAseq dataset from a carcinosarcoma cell culture.

(E) Different EMP states are characterized by the expression of cell surface markers EPCAM, CDH1, ITGB4, and CD200 which demonstrate a gradual loss upon the transition from epithelial to mesenchymal.

(F) Early-passage cell cultures derived from different *K14Cre*$^{Tg/+}$-*R26-ZEB2*$^{Tg/+}$-*Trp53*$^{Fl/Fl}$ mouse tumors show EMP gradients based on the cell surface markers EPCAM, CDH1, ITGB4, and CD200.

overall outcome.[9,24] Mice injected with CD200+ or CD200-cells display macroscopic lung tumors whereas these were not detected in EPCAM+, CDH1+ or ITGB4+ injected mice after 7 weeks (Figures 5B and 5D). Moreover, mice injected with CD200-, CD200+, ITGB4+, CDH1+, and EPCAM+ cells showed a respective median survival of 10.5 ($n = 6$), 11 ($n = 7$), 17 ($n = 7$), 23 ($n = 7$), and 19 ($n = 7$) weeks (Figure 5C). In metastases that developed in tail-vein injected mice, intra-tumor heterogeneity was assessed with KRT14-VIM costainings where we showed that EPCAM+ and CDH1+ injected mice developed predominantly epithelial lung nodules. ITGB4+ injected mice developed E/M mixed lung tumors whereas lung tumors arising from CD200+ and CD200-injected mice largely displayed a mesenchymal VIM+ KRT14-phenotype (Figure 5E).

Since we showed that mesenchymal features in our mixed cSCC model are associated with a higher metastatic capacity and literature describes a strong EMT-chemoresistance association, novel mesenchymal cell-intrinsic vulnerabilities are needed. To this end we treated sorted populations with tumour necrosis factor (TNF) and the SMAC-mimetic BV6 (TB treatment) to induce apoptosis and additionally with the pan-caspase inhibitor zVAD-fmk (TNF+BV6+zVAD-fmk = TBZ treatment) to induce necroptosis.[25] We demonstrated that mesenchymal states (CD200+ and CD200-) are more sensitive to both forms of TNF induced cell death but not ferroptosis induced by Erastin, or the GPX4 inhibitors RSL3 and ML162 (Figure 5F). In the human skin cancer cell lines A431 and COLO16 equipped with an inducible ZEB2 expression construct (Figure S3A),[26] cells which were stimulated with doxycycline for 96 h also displayed higher sensitivity to TB and to a lesser extent, TBZ induced cell death after 24 h (Figure S3B).

Altogether we demonstrated that skin SCC cells with mesenchymal features have a more rapid metastatic progression in experimental metastasis assays yet are more sensitive to TNF-induced cell death.

KLF4, P63, and BHLHE40 dictate epithelial differentiation

To infer the regulatory network underlying the EMP states we applied the single-cell regulatory network inference and clustering (SCENIC) algorithm.[27] The analysis of the *in vivo* MIX tumor and *in vitro* early passage cell culture revealed a strong overlap in transcription factor regulons

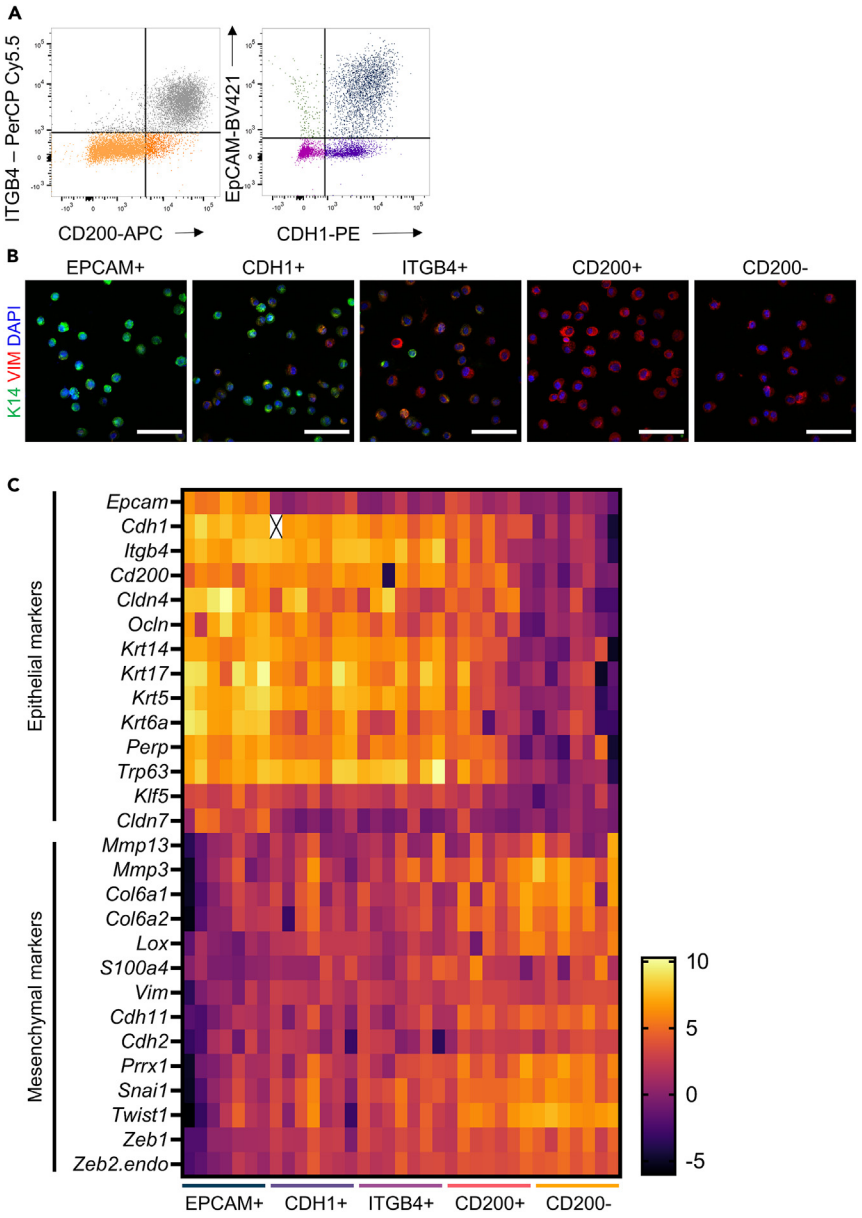

Figure 4. Mixed cSCC lesions exhibit a snapshot of EMP with epithelial, intermediate, and mesenchymal subpopulations

(A) Gating strategy for sorting of the different EMP subpopulations from early-passage cell cultures using FACS.

(B) Keratin 14 (green) and vimentin (red) costainings after cytospin of FACS-sorted EMP subpopulations from mixed cell cultures. Scale bar, 100 μM.

(C) Heatmap with the gene expression of epithelial and mesenchymal markers in sorted EMP states from mixed cell cultures (n = 7) via RT-qPCR.

consisting of *Trp63*, *Klf4*, and *Bhlhe40* within the epithelial compartments (Figure 6A). To functionally validate the importance of epithelial regulon activity, shRNA-mediated knockdown of *Trp63*, *Klf4*, or *Bhlhe40* showed clearly that epithelial differentiation was lost, and cells shifted toward a more mesenchymal phenotype based on *Krt14* and *Vim* (Figures 6B, 6C, and S4A). Moreover, this was accompanied by a shift toward a CD200-phenotype which corresponds with the more mesenchymal states in our proposed EMP model (Figure 6D). To determine whether the loss of epithelial differentiation by knockdown of these TFs also has functional implications, TNF-induced cell death was assessed. Indeed, all three knockdowns resulted in a higher sensitivity to TB and TBZ in accordance with our data from sorted EMP subpopulations (Figure 6E).

DISCUSSION

Conditional expression of the EMP-associated TF ZEB2 in *Krt14Cre*$^{Tg/+}$-*Trp53*$^{Fl/Fl}$ mice, which causes the formation of highly heterogeneous cutaneous squamous cell carcinomas ranging from a mixed E/M phenotype to a fully mesenchymal phenotype. Interestingly, some of these

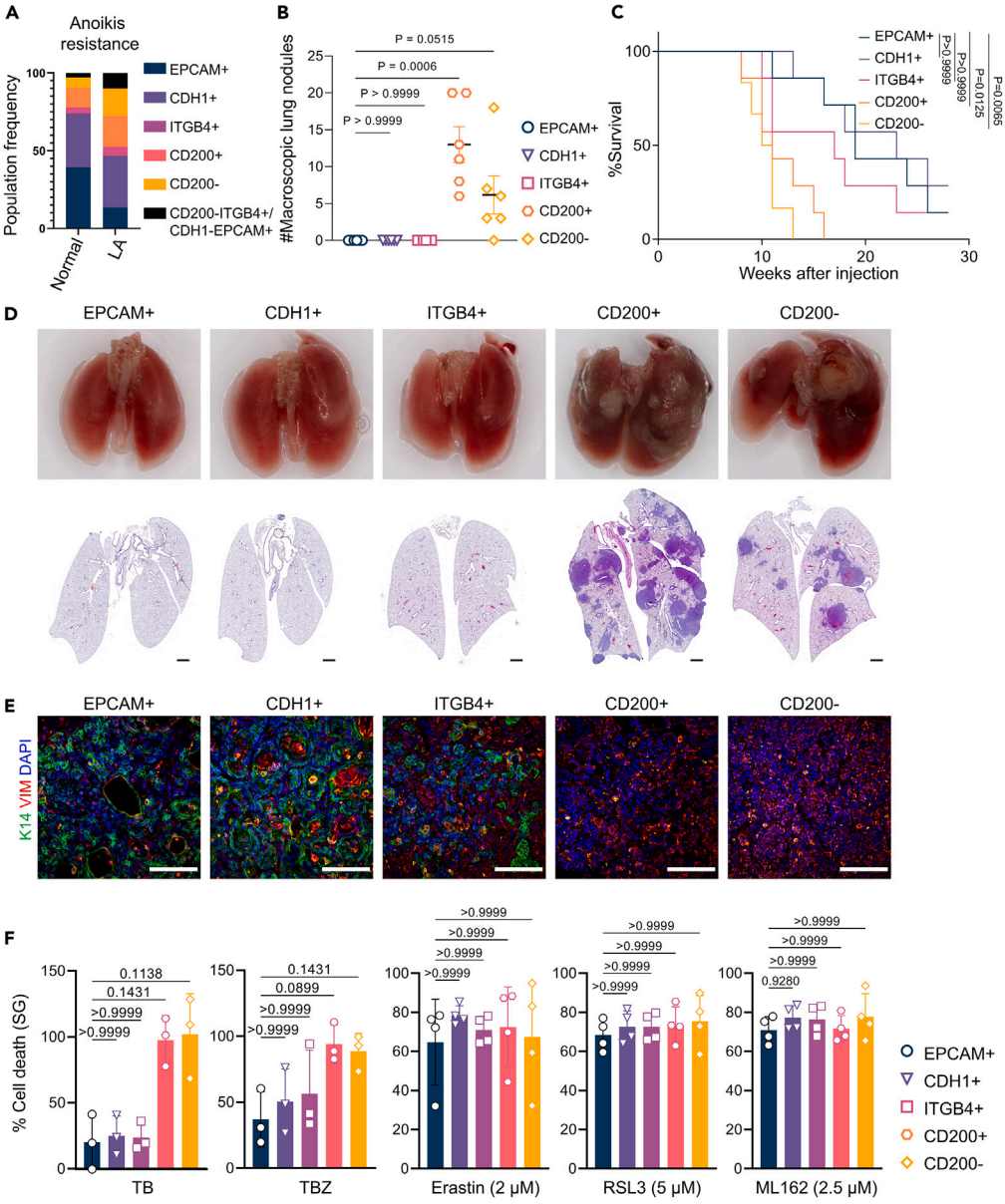

Figure 5. The degree of EMP dictates functional properties in cSCC tumor cells

(A) Anoikis resistance was tested by culturing unsorted cancer cells derived from mixed cell cultures on low-adherence plates and normal plates. Population frequencies were determined after 72 h using EPCAM, CDH1, ITGB4, and CD200 as markers. The experiment was performed in triplicates.

(B) EMP subpopulations were sorted from mixed cell cultures and injected in the tail vein of NOD/SCID/IL2Rγ null mice (n = 6). 6 weeks after injection, macroscopic lung metastases were counted. Statistical significance was determined using a Kruskal-Wallis test followed by a Dunn's multiple comparisons test. Data are represented as mean ± SD.

(C) EMP subpopulations EPCAM+ (N = 7), CDH1+ (N = 7), ITGB4+ (N = 7), CD200+ (N = 7), and CD200- (N = 6) were sorted from mixed cell cultures and injected in the tail vein of NOD/SCID/IL2Rγ null mice. Mice injected with different EMP subpopulations showed a different survival post-injection. Statistical significance was determined using pairwise log rank Mantel-cox tests with mice injected with a fully epithelial (EPCAM) state as a reference group. A Bonferroni correction was used for multiple testing.

(D) Representative macroscope and H&E imaged from lungs isolated from NOD/SCID/IL2Rγ null mice injected with EMT transition states. Scale bar, 1000 μM.

(E) Lung tumors that formed after tail vein injection of sorted EMP subpopulations were stained for KRT14 and VIM. Scale bar, 100 μM.

(F) Cells were sorted based on EPCAM, CDH1, ITGB4, and CD200. Cell death was induced after adherence to the plate with 10 ng/mL TNF, 1 μM BV6 (TB) and 25 μM zVAD FMK (TBZ) (N = 3) or 2 μM Erastin, 5μM RSL3 or 2.5 μM ML162 (N = 4). Cell death was determined after 24 h by SytoxGreen positivity. Statistical significance was determined using a Kruskal-Wallis test followed by a Dunn's multiple comparisons test. Data are represented as mean ± SD.

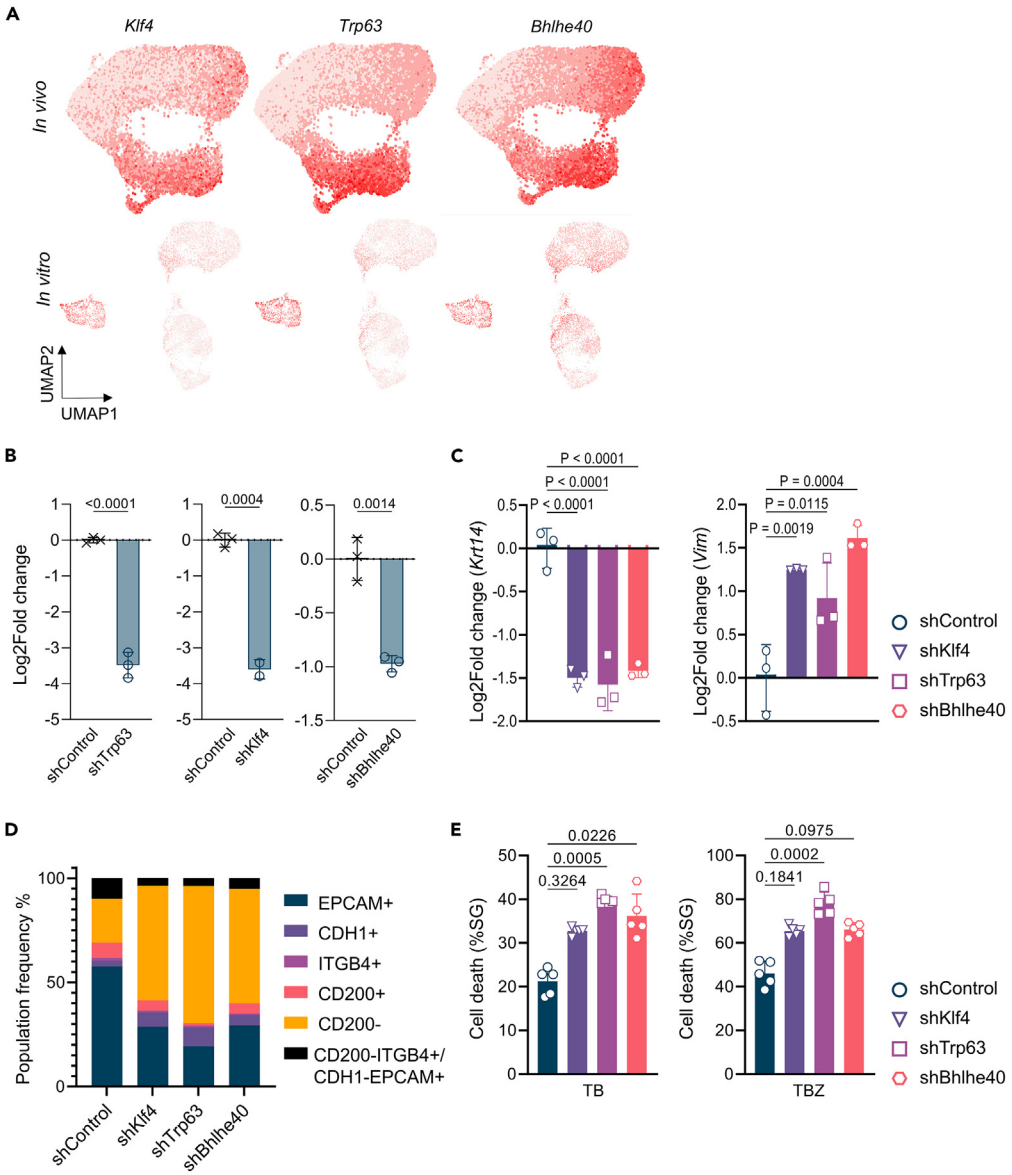

Figure 6. KLF4, P63, and BHLHE40 dictate epithelial differentiation

(A) Area under the curve (AUC) plots for *Klf4*, *Trp63*, and *Bhlhe40* activity in cells from the primary carcinosarcoma tumor and carcinosarcoma-derived cell culture.

(B) Knockdown efficiency of *Trp63*, *Klf4*, and *Bhlhe40* was compared with a non-targeting shRNA (shControl) and validated with RT-qPCR. Statistical significance was determined using an unpaired two-way student t test. Data are represented as mean ± SD.

(C) The relative expression of Krt14 and Vim was determined after *Trp63*, *Klf4*, or *Bhlhe40* knockdown compared to a non-targeting shRNA (shControl) ($N = 3$). Statistical significance was determined using a one-way anova followed by a Dunnett's test. Data are represented as mean ± SD.

(D) The population frequencies of different EMT transition states was determined after knockdown of *Trp63*, *Klf4*, or *Bhlhe40* compared to a non-targeting shRNA (shControl) ($N = 3$).

(E) Cell death was induced after adherence of the cells to the plate with 10 ng/mL TNF, 1 μM BV6 (TB) and 25 μM zVAD FMK (TBZ) ($N = 5$) and determined after 24 h by SytoxGreen positivity. Cell death was compared between cells with a knockdown of *Trp63*, *Klf4*, or *Bhlhe40* and a non-targeting shRNA (shControl). Statistical significance was determined using a Kruskal-Wallis test followed by a Dunn's multiple comparisons test. Data are represented as mean ± SD.

tumors strongly resemble human carcinosarcomas, which are rare tumors with little information on their ontogeny. Mutational profiling of cutaneous carcinosarcomas showed that carcinomatous and sarcomatous compartments comprised mostly identical mutations, which illustrated the monoclonal origin of these lesions.[28] In our study, a KRT14+ epithelial progenitor gives rise to both E and M states in these skin lesions underlying the idea that carcinosarcomas arise from an epithelial progenitor undergoing EMT.

Our results also demonstrated that ZEB2 alone is not responsible for a full dedifferentiation toward a mesenchymal phenotype since all cells, including the epithelial compartment, express the *Zeb2*-transgene. This suggests that ZEB2 drives cells toward a phenotype which is primed to transition and indicates a potential role for the tumor microenvironment in pushing cells to undergo a full mesenchymal differentiation. However, upon cell culturing, cells maintain different EMP phenotypes without microenvironmental cues showing that the TME might drive more outspoken cellular plasticity and in particular cell differentiation in a certain direction, but the maintenance of these phenotypes seems less dependent of the TME.

We have shown the presence of both E and M cells with immunostainings, however, using scRNAseq we identified five distinct cellular states based on the cell surface markers EPCAM, CDH1, ITGB4, and CD200 where a sequential loss of these respective markers was associated with a transition from E to M. The existence of multiple EMP transition states has only recently been investigated with several papers proposing markers to isolate these respective states.[7–10] A recent study has identified that early hybrid EMP phenotypes are more metastatic due to the hypothesis that these have more ability to shift between E and M states.[9] In our model, however, mesenchymal states presented higher experimental metastatic capabilities which coincided with higher *in vitro* anoikis resistance.

While this discrepancy could depend on the model that was used, it should also be noted that the identification of partial states is not an absolute metric. In most studies, partial states are identified based on a relative comparison to epithelial and mesenchymal states within that model. Therefore, the indirect comparison of partial EMT states between models remains difficult as their joined position along the EMT axis is not known. Potentially in our case, the CD200+ or CD200− states could be more heterogeneous and contain different EMP states as well. Partial states within the CD200+ or CD200− phenotype could coincide with partial EMT states from previous reports and drive metastasis.

In literature, mesenchymal features are associated with higher chemoresistance.[29] This coupled with our data which revealed mesenchymal cells to be more metastatic, presents a significant clinical challenge. Therefore new methods for targeting these states should be identified. Here, we explored whether TNF-mediated cell death could selectively kill cell populations with mesenchymal features. Indeed, a higher metastatic capacity fortunately yields cancer cells more sensitivity toward TNF-mediated cell death. This provides opportunities for combination therapies that target both epithelial and mesenchymal cells.

Lastly, we showed that a combination of scRNAseq and algorithms such as SCENIC, which predict regulon activity in cells, can identify transcription factors involved in the EMP process. We identified *Klf4*, *Trp63*, and *Bhlhe40* as regulons that were active in the epithelial compartment of our mixed skin lesions. Although the role for *Klf4* and *Trp63* as epithelial gatekeepers is well established in literature, few publications link *Bhlhe40* to epithelial differentiation.[30–33] Research showed that BHLHE40 competes with SP1 for the SP1 binding site in the TWIST1 promoter in human endometrial cancer, thereby directly influencing EMT.[33] To demonstrate the active involvement of these TFs in maintenance of the epithelial phenotype, we performed shRNA-mediated knockdown. Cells obtained a more mesenchymal state upon knockdown yet these did not reach a complete CD200-phenotype. The combination of a knockdown of multiple TFs or a complete knockout could lead to a stable, fully mesenchymal phenotype. Moreover, these cells obtained higher sensitivity to TNF-mediated cell death. However, to fully capture the complex regulatory network governing EMP in carcinosarcomas and carcinomas, more in depth analysis will need to be performed. This might allow us to drive cells toward a more mesenchymal phenotype which is unfortunately more metastatic but can be readily killed through cell death sensitization.

Altogether, our data demonstrate that ZEB2 plays a crucial role in cSCC development and that these tumors display a snapshot of an ongoing EMP process with 5 distinct cellular states with different degrees of EMP, metastatic capability and cell death sensitivity.

Limitations of the study

In skin SCC, poor differentiation and intra-tumor heterogeneity lower the patients prognosis and relapse. We used a P53 knockout driven by the *Krt14* promoter to induce skin cancer in mice. To drive intratumor heterogeneity a *Zeb2* construct was used. This caused a high degree of heterogeneity that lead to the identification of 5 states; however, the *Zeb2* transgene remains active in all tumor cells. *Zeb2* was inserted in the ROSA26 locus, which has low expression, yet is activated upon tumor ontogeny. A conditional mouse model where *Zeb2* expression is pulsed and not constitutively active could give more insight in how *Zeb2* drives heterogeneity in later stages of tumor development. Due to the limited availability of human carcinosarcoma datasets, we currently lack the ability to map our single cell data on the human pathology to further explore our EMP states.

RESOURCE AVAILABILITY

Lead contact

Further information and any requests for resources and reagents should be directed to and will be fulfilled by the lead contact, Geert Berx (Geert.Berx@ugent.be).

Materials availability

This study did not generate new unique reagents.

Data and code availability

Data reported in this paper wil be shared by the lead contact upon request. The single cell-Rdata generated in this study are publicly available under the accession number GSE265908. This paper does not report original code. Any additional information required to reanalyze the data reported in this paper is available from the lead contact upon request.

ACKNOWLEDGMENTS

G.Berx.'s laboratory is supported by the Geconcerteerde Onderzoeksacties Ghent University (BOF.GOA.2021.0005.02), Kom op tegen Kanker (STI.-DIV.2020.0017.01), Stichting Tegen Kanker (STI.STK.2021.0001.01) and iBOF (BOF.IBO.2023.0005.03). J.V. is supported by a personal PhD fellowship from UGent. K.D.C. received a PhD fellowship from the FWO (2012–2026).

AUTHOR CONTRIBUTIONS

Originators of project: M.T., B.S., N.S., J.V., and G.B. participated in research design: J.V., N.S., M.T., B.D.C., S.G., and G.B. conducted experiments: J.V., N.S., B.S., J.T., M.T., K.B., N.L., K.D.C., and N.V. contributed new reagents or analytic tools: C.V.B., K.V.D.V., J.V.D., and J.H. performed data analysis: J.V., N.S., J.D.C., and N.V. wrote or contributed to the writing of the manuscript: all authors.

DECLARATION OF INTERESTS

The authors declare no competing interests.

STAR★METHODS

Detailed methods are provided in the online version of this paper and include the following:

- KEY RESOURCES TABLE
- EXPERIMENTAL MODEL AND STUDY PARTICIPANT DETAILS
  - Mice
  - Cell lines and culture
- METHOD DETAILS
  - Tumor cell isolation, cell sorting and culturing
  - Flow cytometry and FACS
  - Experimental metastasis assay
  - Anoikis assay
  - Tissue section and immunostaining
  - Immunocytochemistry
  - Western blot analysis
  - Single-cell sequencing analysis
  - Pre-processing data
  - Quantitative RT-PCR
  - Lentiviral transductions for knockdown assays
  - Cell death assay on FLUOstar Omega
- QUANTIFICATION AND STATISTICAL ANALYSIS

SUPPLEMENTAL INFORMATION

Supplemental information can be found online at https://doi.org/10.1016/j.isci.2024.111169.

Received: April 25, 2024
Revised: August 23, 2024
Accepted: October 10, 2024
Published: October 16, 2024

REFERENCES

1. Urban, K., Mehrmal, S., Uppal, P., Giesey, R.L., Delost, G.R., and Heights, M. (2021). The global burden of skin cancer: A longitudinal analysis from the Global Burden of Disease Study, 1990–2017. JAAD Int. *2*, 98–108. https://doi.org/10.1016/J.JDIN.2020.10.013.
2. Sung, H., Ferlay, J., Siegel, R.L., Laversanne, M., Soerjomataram, I., Jemal, A., and Bray, F. (2021). Global Cancer Statistics 2020: GLOBOCAN Estimates of Incidence and Mortality Worldwide for 36 Cancers in 185 Countries. CA. Cancer J. Clin. *71*, 209–249. https://doi.org/10.3322/CAAC.21660.
3. Motaparthi, K., Kapil, J.P., and Velazquez, E.F. (2017). Cutaneous Squamous Cell Carcinoma: Review of the Eighth Edition of the American Joint Committee on Cancer Staging Guidelines, Prognostic Factors, and Histopathologic Variants. Adv. Anat. Pathol. *24*, 171–194. https://doi.org/10.1097/PAP.0000000000000157.
4. Schmults, C.D., Karia, P.S., Carter, J.B., Han, J., and Qureshi, A.A. (2013). Factors predictive of recurrence and death from cutaneous squamous cell carcinoma: A 10-year, single-institution cohort study. JAMA Dermatol. *149*, 541–547. https://doi.org/10.1001/jamadermatol.2013.2139.
5. Mourouzis, C., Boynton, A., Grant, J., Umar, T., Wilson, A., Macpheson, D., and Pratt, C. (2009). Cutaneous head and neck SCCs and risk of nodal metastasis - UK experience. J. Cranio-Maxillo-Fac. Surg. *37*, 443–447. https://doi.org/10.1016/j.jcms.2009.07.007.
6. Thiery, J.P., Acloque, H., Huang, R.Y.J., and Nieto, M.A. (2009). Epithelial-Mesenchymal Transitions in Development and Disease. Cell *139*, 871–890. https://doi.org/10.1016/j.cell.2009.11.007.
7. Ruscetti, M., Quach, B., Dadashian, E.L., Mulholland, D.J., and Wu, H. (2015). Tracking and functional characterization of epithelial-mesenchymal transition and mesenchymal tumor cells during prostate cancer metastasis. Cancer Res. *75*, 2749–2759. https://doi.org/10.1158/0008-5472.CAN-14-3476.
8. Bierie, B., Pierce, S.E., Kroeger, C., Stover, D.G., Pattabiraman, D.R., Thiru, P., Liu Donaher, J., Reinhardt, F., Chaffer, C.L., Keckesova, Z., and Weinberg, R.A. (2017). Integrin-β4 identifies cancer stem cell-enriched populations of partially mesenchymal carcinoma cells. Proc. Natl. Acad. Sci. USA *114*, E2337–E2346. https://doi.org/10.1073/pnas.1618298114.
9. Pastushenko, I., Brisebarre, A., Sifrim, A., Fioramonti, M., Revenco, T., Boumahdi, S., Van Keymeulen, A., Brown, D., Moers, V., Lemaire, S., et al. (2018). Identification of the tumour transition states occurring during EMT. Nature *556*, 463–468. https://doi.org/10.1038/s41586-018-0040-3.
10. Yang, J., Antin, P., Berx, G., Blanpain, C., Brabletz, T., Bronner, M., Campbell, K., Cano, A., Casanova, J., Christofori, G., et al. (2020). Guidelines and definitions for research on epithelial–mesenchymal transition. Nat. Rev. Mol. Cell Biol. *21*, 341–352. https://doi.org/10.1038/s41580-020-0237-9.

11. Grosse-Wilde, A., D'Hérouël, A.F., McIntosh, E., Ertaylan, G., Skupin, A., Kuestner, R.E., Del Sol, A., Walters, K.A., and Huang, S. (2015). Stemness of the hybrid Epithelial/Mesenchymal State in Breast Cancer and Its Association with Poor Survival. PLoS One *10*, e0126522. https://doi.org/10.1371/JOURNAL.PONE.0126522.
12. Verstappe, J., and Berx, G. (2023). A role for partial epithelial-to-mesenchymal transition in enabling stemness in homeostasis and cancer. Semin. Cancer Biol. *90*, 15–28. https://doi.org/10.1016/J.SEMCANCER.2023.02.001.
13. De Craene, B., and Berx, G. (2013). Regulatory networks defining EMT during cancer initiation and progression. Nat. Rev. Cancer *13*, 97–110. https://doi.org/10.1038/nrc3447.
14. Vandewalle, C., Comijn, J., de Craene, B., Vermassen, P., Bruyneel, E., Andersen, H., Tulchinsky, E., van Roy, F., and Berx, G. (2005). SIP1/ZEB2 induces EMT by repressing genes of different epithelial cell-cell junctions. Nucleic Acids Res. *33*, 6566–6578. https://doi.org/10.1093/nar/gki965.
15. Haerinck, J., Goossens, S., and Berx, G. (2023). The epithelial-mesenchymal plasticity landscape: principles of design and mechanisms of regulation. Nat. Rev. Genet. *24*, 590–609. https://doi.org/10.1038/s41576-023-00601-0.
16. Jonkers, J., Meuwissen, R., Van der Gulden, H., Peterse, H., Van der Valk, M., and Berns, A. (2001). Synergistic tumor suppressor activity of BRCA2 and p53 in a conditional mouse model for breast cancer. Nat. Genet. *29*, 418–425. https://doi.org/10.1038/ng747.
17. Colombino, M., Palmieri, G., Rodio, M., Tettamanzi, M., Rampazzo, S., Margani, R., Trignano, E., Cossu, A., Fedeli, M.A., Fadda, G.M., and Rubino, C. (2024). Mutational Profiles of Cutaneous Squamous Cell Carcinomas with Different Patterns of Clinical Aggression from Head and Neck Regions. Cancers *16*, 1956. https://doi.org/10.3390/cancers16111956.
18. Tatari, M.N., de Craene, B., Soen, B., Taminau, J., Vermassen, P., Goossens, S., Haigh, K., Cazzola, S., Lambert, J., Huylebroeck, D., et al. (2014). ZEB2-transgene expression in the epidermis compromises the integrity of the epidermal barrier through the repression of different tight junction proteins. Cell. Mol. Life Sci. *71*, 3599–3609. https://doi.org/10.1007/s00018-014-1589-0.
19. Lengrand, J., Pastushenko, I., Vanuytven, S., Song, Y., Venet, D., Sarate, R.M., Bellina, M., Moers, V., Boinet, A., Sifrim, A., et al. (2023). Pharmacological targeting of netrin-1 inhibits EMT in cancer. Nature *620*, 402–408. https://doi.org/10.1038/s41586-023-06372-2.
20. Smit, M.A., and Peeper, D.S. (2011). Zeb1 is required for TrkB-induced epithelial-mesenchymal transition, anoikis resistance and metastasis. Oncogene *30*, 3735–3744. https://doi.org/10.1038/onc.2011.96.
21. Yu, M., Bardia, A., Wittner, B.S., Stott, S.L., Smas, M.E., Ting, D.T., Isakoff, S.J., Ciciliano, J.C., Wells, M.N., Shah, A.M., et al. (2013). Circulating breast tumor cells exhibit dynamic changes in epithelial and mesenchymal composition. Science (1979) *339*, 580–584. https://doi.org/10.1126/science.1228522.
22. Zhao, R., Cai, Z., Li, S., Cheng, Y., Gao, H., Liu, F., Wu, S., Liu, S., Dong, Y., Zheng, L., et al. (2017). Expression and clinical relevance of epithelial and mesenchymal markers in circulating tumor cells from colorectal cancer. Oncotarget *8*, 9293–9302. https://doi.org/10.18632/ONCOTARGET.14065.
23. Fischer, K.R., Durrans, A., Lee, S., Sheng, J., Li, F., Wong, S.T.C., Choi, H., El Rayes, T., Ryu, S., Troeger, J., et al. (2015). EMT is not required for lung metastasis but contributes to chemoresistance. Nature *527*, 472–476. https://doi.org/10.1038/NATURE15748.
24. Li, Y., Lv, Z., Zhang, S., Wang, Z., He, L., Tang, M., Pu, W., Zhao, H., Zhang, Z., Shi, Q., et al. (2020). Genetic Fate Mapping of Transient Cell Fate Reveals N-Cadherin Activity and Function in Tumor Metastasis. Dev. Cell *54*, 593–607.e5. https://doi.org/10.1016/j.devcel.2020.06.021.
25. Grootjans, S., Hassannia, B., Delrue, I., Goossens, V., Wiernicki, B., Dondelinger, Y., Bertrand, M.J.M., Krysko, D.V., Vuylsteke, M., Vandenabeele, P., and Vanden Berghe, T. (2016). A real-time fluorometric method for the simultaneous detection of cell death type and rate. Nat. Protoc. *11*, 1444–1454. https://doi.org/10.1038/nprot.2016.085.
26. Skrypek, N., Bruneel, K., Vandewalle, C., De Smedt, E., Soen, B., Loret, N., Taminau, J., Goossens, S., Vandamme, N., and Berx, G. (2018). ZEB2 stably represses RAB25 expression through epigenetic regulation by SIRT1 and DNMTs during epithelial-to-mesenchymal transition. Epigenet. Chromatin *11*, 70. https://doi.org/10.1186/s13072-018-0239-4.
27. Aibar, S., González-Blas, C.B., Moerman, T., Huynh-Thu, V.A., Imrichova, H., Hulselmans, G., Rambow, F., Marine, J.C., Geurts, P., Aerts, J., et al. (2017). SCENIC: Single-cell regulatory network inference and clustering. Nat. Methods *14*, 1083–1086. https://doi.org/10.1038/nmeth.4463.
28. Paniz-Mondolfi, A., Singh, R., Jour, G., Mahmoodi, M., Diwan, A.H., Barkoh, B.A., Cason, R., Huttenbach, Y., Benaim, G., Galbincea, J., and Luthra, R. (2014). Cutaneous carcinosarcoma: further insights into its mutational landscape through massive parallel genome sequencing. Virchows Arch. *465*, 339–350. https://doi.org/10.1007/s00428-014-1628-0.
29. Shibue, T., and Weinberg, R.A. (2017). EMT, CSCs, and drug resistance: the mechanistic link and clinical implications. Nat. Rev. Clin. Oncol. *14*, 611–629. https://doi.org/10.1038/nrclinonc.2017.44.
30. Latil, M., Nassar, D., Beck, B., Boumahdi, S., Wang, L., Brisebarre, A., Dubois, C., Nkusi, E., Lenglez, S., Checinska, A., et al. (2017). Cell-Type-Specific Chromatin States Differentially Prime Squamous Cell Carcinoma Tumor-Initiating Cells for Epithelial to Mesenchymal Transition. Cell Stem Cell *20*, 191–204.e5. https://doi.org/10.1016/j.stem.2016.10.018.
31. Subbalakshmi, A.R., Sahoo, S., McMullen, I., Saxena, A.N., Venugopal, S.K., Somarelli, J.A., and Jolly, M.K. (2021). KLF4 Induces Mesenchymal-Epithelial Transition (MET) by Suppressing Multiple EMT-Inducing Transcription Factors. Cancers *13*, 5135. https://doi.org/10.3390/cancers13205135.
32. Tiwari, N., Meyer-Schaller, N., Arnold, P., Antoniadis, H., Pachkov, M., van Nimwegen, E., and Christofori, G. (2013). Klf4 is a transcriptional regulator of genes critical for EMT, including Jnk1 (Mapk8). PLoS One *8*, e57329. https://doi.org/10.1371/journal.pone.0057329.
33. Asanoma, K., Liu, G., Yamane, T., Miyanari, Y., Takao, T., Yagi, H., Ohgami, T., Ichinoe, A., Sonoda, K., Wake, N., and Kato, K. (2015). Regulation of the Mechanism of TWIST1 Transcription by BHLHE40 and BHLHE41 in Cancer Cells. Mol. Cell Biol. *35*, 4096–4109. https://doi.org/10.1128/MCB.00678-15.
34. Moore, G.E., Merrick, S.B., Woods, L.K., and Arabasz, N.M. (1975). A human squamous cell carcinoma cell line. Cancer Res. *35*, 2684–2688.
35. Schneider, C.A., Rasband, W.S., and Eliceiri, K.W. (2012). NIH Image to ImageJ: 25 years of Image Analysis. Nat. Methods *9*, 671–675. https://doi.org/10.1038/NMETH.2089.
36. Bankhead, P., Loughrey, M.B., Fernández, J.A., Dombrowski, Y., McArt, D.G., Dunne, P.D., McQuaid, S., Gray, R.T., Murray, L.J., Coleman, H.G., et al. (2017). QuPath: Open source software for digital pathology image analysis. Sci. Rep. *7*, 16878. https://doi.org/10.1038/S41598-017-17204-5.
37. Stuart, T., Butler, A., Hoffman, P., Hafemeister, C., Papalexi, E., Mauck, W.M., Hao, Y., Stoeckius, M., Smibert, P., and Satija, R. (2019). Comprehensive Integration of Single-Cell Data. Cell *177*, 1888–1902.e21. https://doi.org/10.1016/J.CELL.2019.05.031.
38. Korsunsky, I., Millard, N., Fan, J., Slowikowski, K., Zhang, F., Wei, K., Baglaenko, Y., Brenner, M., Loh, P.R., and Raychaudhuri, S. (2019). Fast, sensitive, and accurate integration of single cell data with Harmony. Nat. Methods *16*, 1289–1296. https://doi.org/10.1101/461954.

STAR★METHODS

KEY RESOURCES TABLE

REAGENT or RESOURCE	SOURCE	IDENTIFIER
Antibodies		
Rat monoclonal CD200 (OX2) - APC (clone OX-90)	Biolegend	Cat#123810; RRID: AB_10900447
Rat monoclonal CD104 - PerCp/Cy5.5 (clone 346-11A)	Biolegend	Cat#123614; RRID: AB_2734184
Rat monoclonal CD324 (E-cadherin) - PE (clone DECMA-1)	Biolegend	Cat#147304; RRID: AB_2563040
Rat monoclonal CD326 (Ep-Cam) - BV421 (clone G8.8)	Biolegend	Cat#118225; RRID: AB_2563983
Rabbit monoclonal vimentin (clone EPR3776)	Abcam	Cat#ab92547; RRID: AB_10562134
Chicken polyclonal vimentin	Novus biologicals	Cat#NB300-223SS; RRID: AB_922758
Mouse monoclonal E-cadherin (clone 36)	BD Transduction Laboratories	Cat#610181, RRID: AB_397580
Rabbit monoclonal GFP (clone D5.1)	Cell Signalling Technology	Cat#2956, RRID: AB_1196615
Mouse monoclonal cytokeratin 14 (clone LL002)	Abcam	Cat#ab7800, RRID: AB_306091
Mouse monoclonal anti-ZEB2 (7B7)	Protein service facility VIB	N/A
Pan-cytokeratin	Abcam	Cat#Ab215838, RRID: AB_2922672
DEC1	Novus biologicals	Cat#NB100-1800SS, RRID: AB_1852832
Mouse Anti-p63 Monoclonal Antibody, Unconjugated, Clone BC4A4	Abcam	Cat#ab735, RRID: AB_305870
KLF4	Cell signalling technolgy	Cat#4038, RRID: AB_2265207
Chemicals, peptides, and recombinant proteins		
Collagenase A	Roche	Cat#10103586001
Dispase II	Roche	Cat#04942078001
DNAse I	Roche	Cat#04536282001
Dulbecco's Modified Eagle Medium (DMEM)	Gibco	Cat#41965-039
NA-Pyruvate	Sigma	Cat#S-8636
Non-essential amino acids	Gibco	Cat#11140-035
Penicillin/streptomycin	Sigma	Cat#P-4333
EDTA	VWR	Cat#PRO20302.293
Trypsin	Sigma	Cat#T-4424
Goat serum	Gibco	Cat#16210-064
Bovine serum albumin	VWR	Cat#0332
BV6	Selleckchem	Cat#S7597
Erastin	Selleckchem	Cat#HY-15763
zVAD FMK	Selleckchem	Cat#S7023
RSL3	Selleckchem	Cat#S8155
ML162	Selleckchem	Cat#SML2561
SytoxGreen	Invitrogen	Cat#S7020
TNF	VIB Protein Service Facility	N/A
Critical commercial assays		
SensiFast SYBR No-Rox Kit	Bioline	Cat#CSA-01190

(*Continued on next page*)

Continued

REAGENT or RESOURCE	SOURCE	IDENTIFIER
Sensifast cDNA Synthesis Kit	Bioline	Cat#BIO-650504
Deposited data		
Analyzed dataset	Lengrand et al.[19]	GEO:GSE234267
Single cell RNA sequencing datasets	This paper	GEO:GSE265908
Experimental models: Cell lines		
A431	ATCC	RRID:CVCL_0037
COLO16	Moore et al.[34]	RRID:CVCL_D607
Experimental models: Organisms/strains		
NOD.Cg-*Prkdc*^{scid} *Il2rg*^{tm1Wjl}/SzJ	005557	The Jackson Laboratory
Oligonucleotides		
Bhlhe40 - qPCR FWD	IDT	ACGGAGACCTGTCAGGGATG
Bhlhe40 - qPCR REV	IDT	GGCAGTTTGTAAGTTTCCTTGC
Cd200 - qPCR FWD	IDT	CTCTCCACCTACAGCCTGATT
Cd200 - qPCR REV	IDT	AGAACATCGTAAGGATGCAGTTG
Cdh1 - qPCR FWD	IDT	TGCCATCCTCGGAATCCTT
Cdh1 - qPCR REV	IDT	GGCTCTTTGACCACCGTTCTC
Cdh11 - qPCR FWD	IDT	CTGGGTCTGGAACCAATTCTTT
Cdh11 - qPCR REV	IDT	GCCTGAGCCATCAGTGTGTA
Cdh2 - qPCR FWD	IDT	CCAGGTTTGGAATGGGTCTGT
Cdh2 - qPCR REV	IDT	GTACCGCAGCATTCCATTCA
Cldn4 - qPCR FWD	IDT	ACCCACCCACCTACCCTACTA
Cldn4 - qPCR REV	IDT	TCCCCAGCCCTCCCCAAACCA
Cldn7 - qPCR FWD	IDT	GGCCTGATAGCGAGCACTG
Cldn7 - qPCR REV	IDT	TGGCGACAAACATGGCTAAGA
Col6a1 - qPCR FWD	IDT	CTGCTGCTACAAGCCTGCT
Col6a1 - qPCR REV	IDT	CCCCATAAGGTTTCAGCCTCA
Col6a2 - qPCR FWD	IDT	AAGGCCCCATTGGATTCCC
Col6a2 - qPCR REV	IDT	CTCCCTTCCGACCATCCGAT
Eef1a1 - qPCR FWD	IDT	TCGCCTTGGACGTTCTTTT
Eef1a1 - qPCR REV	IDT	GTGGACTTGCCGGAATCTAC
Epcam - qPCR FWD	IDT	GCGGCTCAGAGAGACTGTG
Epcam - qPCR REV	IDT	CCAAGCATTTAGACGCCAGTTT
Gadph - qPCR FWD	IDT	CATGGCCTTCCGTGTTCCTA
Gadph - qPCR REV	IDT	CCTGCTTCACCACCTTCTTGAT
Hprt - qPCR FWD	IDT	TGCTCGAGATGTCATGAAGG
Hprt - qPCR REV	IDT	AATCCAGCAGGTCAGCAAAG
Itgb4 - qPCR FWD	IDT	ACTCCATGTCTGACGATCTGG
Itgb4 - qPCR REV	IDT	GGGACGCTGACTTTGTCCAC
Klf4 - qPCR FWD	IDT	GTGCCCCGACTAACCGTTG
Klf4 - qPCR REV	IDT	GTCGTTGAACTCCTCGGTCT
Klf5 - qPCR FWD	IDT	GGCTCTCCCCGAGTTCACTA
Klf5 - qPCR REV	IDT	ATTACTGCCGTCTGGTTTGTC
Krt14 - qPCR FWD	IDT	GTCATGGATGTGCACGATGG
Krt14 - qPCR REV	IDT	CCTCCTAAGCCTGAGCAGCAT

(*Continued on next page*)

Continued

REAGENT or RESOURCE	SOURCE	IDENTIFIER
Krt17 - qPCR FWD	IDT	ACCATCCGCCAGTTTACCTC
Krt17 - qPCR REV	IDT	CTACCCAGGCCACTAGCTGA
Krt5 - qPCR FWD	IDT	CTGAGGTCAAGGCCCAGTATG
Krt5 - qPCR REV	IDT	TTGGTGTTGCGGAGGTCAT
Krt6a - qPCR FWD	IDT	GCCCTGCCGTTTCTCTACTTC
Krt6a - qPCR REV	IDT	CGGTGGCTGGTTTGACTTTT
Lox - qPCR FWD	IDT	TCTTCTGCTGCGTGACAACC
Lox - qPCR REV	IDT	GAGAAACCAGCTTGGAACCAG
Matr3 - qPCR FWD	IDT	TGGACCAAGAGGAAATCTGG
Matr3 - qPCR REV	IDT	TGAACAACTCGGCTGGTTTC
Mmp13 - qPCR FWD	IDT	CTTCTTCTTGTTGAGCTGGACTC
Mmp13 - qPCR REV	IDT	CTGTGGAGGTCACTGTAGACT
Mmp3 - qPCR FWD	IDT	ATGGCCTTGCAAAAGATGTGA
Mmp3 - qPCR REV	IDT	TCCAACCCGAGGAACTTCTG
Perp - qPCR FWD	IDT	ATCGCCTTCGACATCATCGC
Perp - qPCR REV	IDT	CCCCATGCGTACTCCATGAG
Prrx1 - qPCR FWD	IDT	GAGCGTGTCTTTGAGCGGA
Prrx1 - qPCR REV	IDT	CATGTGGCAGAATAAGTAGCCAT
Rpl13a - qPCR FWD	IDT	CCTGCTGCTCTCAAGGTTGTT
Rpl13a - qPCR REV	IDT	TGGTTGTCACTGCCTGGTACTT
S100a4 - qPCR FWD	IDT	TCCACAAATACTCAGGCAAAGAG
S100a4 - qPCR REV	IDT	GCAGCTCCCTGGTCAGTAG
Sdha - qPCR FWD	IDT	TACCCGGAATTTCAGAGACG
Sdha - qPCR REV	IDT	CCACCCATGTTGTAATGCAC
Snai1 - qPCR FWD	IDT	CGGAAGCCCAACTATAGCGA
Snai1 - qPCR REV	IDT	GGTCGTAGGGCTGCTGGAA
Trp63 - qPCR FWD	IDT	CAAAACCCTGGAAGCAGAAA
Trp63 - qPCR REV	IDT	GAGGAGCCGTTCTGAATCTG
Twist1 - qPCR FWD	IDT	GGCTCAGCTACGCCTTCTC
Twist1 - qPCR REV	IDT	CATTTTCTCCTTCTCTGGAAACA
Vim - qPCR FWD	IDT	TGGTTGACACCCACTCAAAA
Vim - qPCR REV	IDT	GGTCATCGTGATGCTGAGAA
Ywhaz - qPCR FWD	IDT	TGACACTGGGCAGCATTAAC
Ywhaz - qPCR REV	IDT	GCCCAACATGGAAATAGAGG
Zeb1 - qPCR FWD	IDT	TTGCGTGTCAGGCATGGAT
Zeb1 - qPCR REV	IDT	GAAAACGGCTGTGAACCAAAA
Zeb2 - qPCR FWD	IDT	CAACACTTTCCTTTCGCTATTC
Zeb2 - qPCR REV	IDT	CTTCACATCCAGGTCACTTT
Klf4	BCCM/GeneCorner	GCGTGAGGAACTCTCTCACAT
Trp63	BCCM/GeneCorner	CCCAGTCATCTGATTCGAGTA
Bhlhe40	BCCM/GeneCorner	CTGGTGATTTGTCGGGAAGAA
Recombinant DNA		
MISSION® pLKO.1-puro Non-Mammalian shRNA Control Plasmid DNA	Sigma-Aldrich	SHC002

(*Continued on next page*)

Continued

REAGENT or RESOURCE	SOURCE	IDENTIFIER
Software and algorithms		
FlowJo	FlowJo	https://www.flowjo.com
GraphPad Prism 9	Graphpad	https://www.graphpad.com/
qBase+	Cellcarta	–
SCENIC	Aibar et al.[27]	https://github.com/aertslab/SCENIC
ImageJ	Schneider et al.[35]	https://imagej.nih.gov/ij
Qupath	Bankhead et al.[36]	https://qupath.github.io/
Seurat (V 3.1.2)	Stuart et al.[37]	https://github.com/satijalab/seurat/releases/tag/v3.0.0
Harmony	Korsunsky et al.[38]	https://github.com/immunogenomics/harmony

EXPERIMENTAL MODEL AND STUDY PARTICIPANT DETAILS

Mice

K14Cre$^{Tg/+}$-*Rosa26-Zeb2*$^{Tg/+}$-*Trp53*$^{Fl/Fl}$ mice were generated by crossing *K14Cre*$^{Tg/+}$-*Rosa26-Zeb2*$^{Tg/Tg}$ and *K14Cre*$^{Tg/+}$-*Trp53*$^{Fl/Fl}$ mice (Tatari, 2014, Jonkers, 2001, Derksen, 2006). NOD/SCID/IL2Rγ null mice were purchased from (The Jackson laboratory). The mice used in this study were composed of both males and females with mixed genetic backgrounds. All mice were bred and maintained at the VIB (Ghent University) under specific pathogen free conditions. All experiments were performed in accordance with the ethical committee of the Faculty of Sciences, UGent and VIB.

Cell lines and culture

A431 and Colo16 were lentivirally transduced with a pSIN-hZEB2-3xHA-puro plasmid (Experimental procedure described under "lentiviral transductions for knockdown assays"). Cells were cultured in DMEM supplemented with 10% FBS, penicillin/streptomycin, non-essential amino acids, and Na-pyruvate at 37°C under 5% CO_2.

METHOD DETAILS

Tumor cell isolation, cell sorting and culturing

The tumors developed in *K14Cre*$^{Tg/+}$-*Rosa26-Zeb2*$^{Tg/+}$-*Trp53*$^{Fl/Fl}$ mice were dissected, measured, finely chopped, and digested in 2 mg/ml collagenase A (Roche), 0.125 U/ml dispase II (Roche) and 1 μg/ml DNAse I (Roche) for 1 h at 37°C with gentle agitation. The digested tumor was passed through a 100-μm cell strainer, and the cells were washed in PBS containing 2% FCS. The cell suspension was stained DAPI for 1 h at 4°C. Tumor cells were sorted on a BD FACS ARIA II (BD bioscience) by forward and side scatter, doublet discrimination and DAPI exclusion. Tumor cells were selected by GFP positivity. The GFP+ tumor cells were cultured in DMEM supplemented with 10% FCS, penicillin/streptomycin, non-essential amino acids, and Na-pyruvate at 37°C under 5% CO_2.

Flow cytometry and FACS

Cells were detached using trypsin-EDTA, stained during 40 mins in PBS + 2% FCS, washed and loaded on the BD FACS symphony S6. Cell viability was checked using fixable viability dye eFluor780 (Thermo Fisher). Antibodies can be found in the key resources table.

Experimental metastasis assay

Sorted cells were collected in PBS + 2% FCS at 4°C. 150 000 cells were resuspended in 150 μl PBS and injected in the tail vein of NOD/SCID/IL2Rγ null mice. Mice were sacrificed upon reaching humane endpoints (weight loss of 20% or general signs of disease). Lungs were harvested and used for immunohistochemistry as described in "tissue section and immunostaining".

Anoikis assay

Cells were incubated on an Ultra-Low Attachment 24 well plate (3473, Costar) or a TC-treated 24 well plate (734-2325, VWR) for 72 hours after which flow cytometry was performed against EPCAM, CDH1, ITGB4 and CD200. Antibodies can be found in the key resources table.

Tissue section and immunostaining

All stainings were performed on paraffin sections. Tumor tissues were pre-fixed in 4% paraformaldehyde overnight at room temperature and incubated in 70% ethanol for 24 h before embedding in paraffin. Tissues were cut into 3-μm sections. After deparaffinization, antigens were retrieved in Retrieval buffer pH 9 (Agilent Dako) in a pressure cooker for 2 h. To reduce autofluorescence, tissues were incubated in 0.25% NH_3 in 70% ethanol for 1 h at room temperature, followed by 50% ethanol for 10 min and rinsed twice in PBS. Tissues were blocked with 10% goat

serum diluted in PBS with 1% BSA and 0.1% Tween-20 for 1 h at room temperature. Primary antibodies were incubated overnight at 4°C in the dilution buffer (10% goat serum diluted in PBS with 1% BSA). Tissues were washed three times in PBS for 5 min and incubated with secondary antibodies in the dilution buffer for 1 h at room temperature in the dark. Nuclei were stained with DAPI. To reduce autofluorescence, tissue sections were immersed in 0.3% Sudan black in 70% ethanol for 1 h at room temperature and washed extensively in PBS. The slides were mounted with polyvinyl alcohol mounting medium with DABCO (10981-100ML). Slides were imaged using an LSM880 confocal microscope (Zeiss) or AxioScan (Zeiss) and analysed using ImageJ or QuPath.[35,36] Antibodies can be found in the key resources table.

Immunocytochemistry

Cells were seeded on an eight-well Permanox plastic slide and grown to 70% confluence. Cells were fixed in 4% paraformaldehyde for 1 h at 37°C and washed three times with PBS. Permeabilization and blocking steps were performed simultaneously with PBS containing 10% goat serum, 1% BSA and 0.1% Tween-20 for 1 h at room temperature. Cells were washed three times with PBS for 5 min and incubated with primary antibodies in the dilution buffer overnight at 4°C. Three washing steps were performed with PBS followed by incubation with secondary antibodies in the dilution buffer for 1 h at room temperature in the dark. Nuclei were stained with DAPI. Finally, cells were washed three times in PBS and the slides were mounted with polyvinyl alcohol mounting medium with DABCO (10981-100ML). Slides were imaged using an LSM880 confocal microscope (Zeiss) and analysed using ImageJ.[35] Antibodies can be found in the key resources table.

Western blot analysis

Cells were washed in ice-cold PBS and lysed in NP-40 lysis buffer (10% glycerol, 1% NP-40, 150 mM NaCl and 10 mM Tris-HCl pH 8 supplemented with phosphatase and protease inhibitor cocktail tablets (Roche Diagnostics)). 20 μg of protein was separated on a acrylamide gel and transferred to a polyvinylidene difluoride membrane. Membranes were incubated with primary antibodies and appropriate HRP-labeled secondary antibodies (GE Healthcare). Primary antibodies were diluted in 5% milk. Detection was performed with the Immobilion Western HRP Substrate (Millipore).

Single-cell sequencing analysis

Cells were loaded on a GemCode Single-Cell instrument (10x Genomics) to generate single cell gel bead-in-emulsion (GEM). Single cell libraries were prepared with GemCode Single-Cell instrument (10x Genomics) according to the manufacturer's recommendations.

Library prep was performed by the VIB Single Cell Core (VIB, Ghent-Leuven, Belgium). Sequencing libraries were loaded at 2.1pM loading concentration on a HiSeq4000 with custom sequencing metrics (single-indexed sequencing run, 28/8/0/98 cycles for R1/i7/i5/R2) (Illumina). Sequencing was performed at the VIB Nucleomics Core (VIB, Leuven, Belgium). Demultiplexing was done with 10X CellRanger software (10x Genomics, Cellranger mkfastq). Obtained FASTQ read files were used as input for the CellRanger count pipeline (v 4.0.0) which performs alignment against mouse reference genome (GRCm38), filtering of empty barcodes and counting of unique molecular identifier (UMI).

Pre-processing data

All pre-processing after CellRanger was assessed using R version 3.6.0 (2019-04-26). The raw gene expression matrix from the CellRanger pipeline was filtered, normalized and clustered by using the Seurat (v 3.1.2) pipeline.[37] Filtering was performed on the raw gene expression matrix of all individual samples. Cells were filtered out based on following criteria: > 1000 unique molecular identifiers (UMI); > 200 genes and < 8,000 genes; < 20% percentage of mitochondrial genes expressed. After removing cells not matching these criteria, we used Seurat to normalize the data to the natural log, detected the top 2,000 highly variable genes with the variance stabilizing transformation (vst) method as implemented in the FindVariableFeatures function. Scaling of the highly variable genes was performed using the ScaleData function. By performing principal component analysis, we reduced the dimensionality of the data using the highly variable genes. Clustering was performed using the nearest neighbour method as implemented in Seurat and visualized with Uniform Manifold Approximation and Projection (UMAP). Additionally, we removed cell clusters containing contaminating populations such as fibroblasts and endothelial cells based on their well defined publicly available markers (*Col1a2*, *Col1a1*, *Fap*) and *Pecam1* resepectively. Finally, we re-clustered the data and obtained 7,144, 16,135 and 13, 349 cells respectively for CCL, MIX and MSL samples.

Due to differences in sequencing depth between the MIX and MSL tumors, we used harmony as a batch correction method when integrating both datasets.[38] Harmony was run with standard parameters including the group.by.vars parameter that was set to tumor origin. The R package version 0.99.9 was used.

Identification of the five subpopulations in the CCL single-cell RNA sequencing data was assessed using a subclustering of the epithelial (EP) cluster and the expression of Cd200. In the subclustering, we increased the resolution to 2 in order to identify more diverse subpopulations. We annotated the diverse populations based on the following markers: *Epcam*, *Cdh1*, *Itgb4*. Next, we determined the z-scores of *Cd200* across all cells (EP+MES) and classified the *Cd200*+ cells with a z-score > 0. All other cells were classified as *Cd200*-. Differential gene expression of the five subpopulations was assessed with the FindMarkers function within Seurat using the wilcox test. Genes were filtered with adjusted p value < 0.05 and |log2FC| > 0.25 (Table S1).

Processing of the scRNAseq data from the published *Lgr5-cre^{ER};Kras^{G12D} ;Trp53^{cKO} ;Rosa-YFP* (LKPR) (GSE234267) was performed as described in Lengrand et al. 2023.[19] YFP+ tumor cells were clustered from both control and NP137-treated mice and integrated using harmony.

Quantitative RT-PCR

Total RNA was prepared from cells using the Nucleospin RNA Plus 250 kit (Macherey-Nagel) and cDNA was prepared with SensiFast™ cDNA synthesis kit (Bioline) following manufacturer's recommendations. Quantitative PCR was performed using a SensiFAST™ SYBR® No-Rox kit (GeC Biotech) following manufacturer's recommendations in a LightCycler® 480 (Roche Diagnostics) and analysed with the qBase+ software (Biogazelle). Primer information can be found in the key resources table. The expression levels of the genes of interest were normalized to the housekeeping genes *Ywhaz*, *Gadph*, *Sdha*, *Hprt*, *Eef1a1*, *Matr3* and *Rpl13*.

Lentiviral transductions for knockdown assays

To knockdown *Klf4*, *Trp63* and *Bhlhe40*, lentiviral transductions were performed. Virus was produced in HEK293T cells via calcium phosphate transfection of psPAX2 (packaging plasmid), pMD2.G (envelope plasmid) and pLKO1.5 (shRNA containing plasmid) plasmids. Transduced cells were selected with 1.5 μg/ml puromycin. The Sigma MISSION TRCN clones were supplied by BCCM/GeneCorner. shRNA sequences can be found in the key resources table.

Cell death assay on FLUOstar Omega

Cell lines derived from murine skin tumors were sorted (indicated in figures) and seeded at 10000 cells per well in 96 well plates and induced for cell death upon attachment. A431 iZEB2 cells were seeded at 5000 cells/well and pretreated with doxycycline for 72h. Cell death was induced with 10 ng/ml TNF (VIB Protein Service Facility), 1 μM BV6 (S7597, Selleckchem) and 25 μM zVAD FMK (S7023, Selleckchem) or 2 μM Erastin (HY-15763, Selleckchem), 5 μM RSL3 (S8155, Selleckchem) or 2,5 μM ML162 (SML2561, Sigma-Aldrich) in combination with 5μM SytoxGreen (S7020, Invitrogen). Sytox green intensity was measured after 24h (excitation 485 nm, emission 520 nm) on the Fluostar Omega Microplate reader (BMG LABTECH, Offenburg, Germany) with an excitation filter of 485 nm, emission filter of 520 nm, gains set at 1000, 10 flashes per well and orbital averaging with a diameter of 4 mm. The percentage of cell death was calculated by subtracting the background fluorescence from the induced SytoxGreen fluorescence and dividing this by the maximal fluorescence after subtraction of the background fluorescence. Maximal fluorescence was obtained through cell permeabilization by 0.05% Triton X-100.

QUANTIFICATION AND STATISTICAL ANALYSIS

All statistical analyses were performed using Graphpad Prism 9. The statistical tests that were used are mentioned in the figure legends. Statistical significance for qRT-PCR experiments were performed with a one-way Anova followed by a Tukey's test when comparing more than 2 groups or an unpaired two-way student T-test for comparing two groups. Statistical significance for survival analyses was determined via a log-rank Mantel-cox test. For all other experiments, statistical significance was determined using a kruskal-wallis test followed by a Dunn's multiple comparisons test when comparing more than two groups and a mann-whitney U test for comparison between two groups.